JOURNAL OF PROPULSION AND POWER
Vol. 22, No. 2, March–April 2006

Rotating Stall Control in Axial Compressor Subject to Wheel Speed Transients

Craig A. Buhr,* Matthew A. Franchek,† and Sanford Fleeter‡
Purdue University, West Lafayette, Indiana 47907

A gain-scheduled controller design methodology for rotating stall control in an axial flow compressor subject to wheel speed transients is presented. Linear robust controllers are designed for a family of flow coefficients in the spatial domain at specified discrete wheel speeds to regulate nonaxisymmetric flow. The resulting family of controllers are then gain scheduled with respect to wheel speed in an effort to address the transient wheel speed condition. To validate the performance of the gain schedule control law, domains of attraction obtained from initial condition simulated responses of the nonlinear compressor model are used.

I. Introduction

ROTATING stall and surge are aerodynamic instabilities that occur during operation of a compressor near the peak pressure rise of the compressor. These instabilities degrade performance and produce large loading effects on the compressor blades. To avoid the occurrence of these flow instabilities, the compressor is operated at conditions that are removed from the surge line (stability line), thus creating a factor of safety defined as the surge margin. The surge margin required to prevent the occurrence of rotating stall and surge during wheel speed transients is related to the rate of change of the wheel speed.[1] Therefore, a tradeoff is made between the size of the surge margin and the rate at which the wheel speed may be changed. The goal of active control is to alleviate this tradeoff through simultaneously controlling both wheel speed and rotating stall/surge as shown in Fig. 1. Possible approaches for this control problem include Lyapunov methods (see Ref. 2) and gain-scheduled control (see Refs. 3 and 4).

Successful surge and speed control laws have been developed for one-dimensional centrifugal compressor models with nonconstant impeller speed using Lyapunov methods (see Refs. 5 and 6). For example, Gravdahl[5] developed control laws for surge and wheel speed. The surge control law used a close-coupled valve for actuation. Using Lyapunov's method, he was able to prove semiglobal exponential stability for the surge control law with a proportional–integral speed control law. The control law was validated through simulation. In Ref. 6, Leonessa et al. proposed a nonlinear switching-based framework for surge control utilizing a bleed valve for actuation. Subcontrollers are designed for local set points parameterized by the equilibrium manifold using equilibrium-dependent Lyapunov functions. The local set points are chosen such that they are in the domain of attraction of a neighboring operating point. Therefore, by appropriately switching controllers, stable transitions are ensured.

Badmus et al.[7] achieved rotating stall avoidance and surge control over a range of compressor operation despite inlet/outlet pressure disturbances and variations in commanded mass flow and compressor speed using a gain-scheduling approach. A two-degree-of-freedom gain-scheduled controller was designed using a linearized one-dimensional axial compressor model with a bleed valve for actuation. The controllers are continuously scheduled based on the operating point and achieved rotating stall and surge control over a range of compressor operation despite inlet/outlet pressure disturbances and variations in commanded mass flow and compressor speed. Each of control schemes presented in Refs. 5–7 focused on the control of surge using a one-dimensional compressor model for the analysis and controller design. In contrast, the focus in this paper is the control of rotating stall during wheel speed transients. Because rotating stall is inherently a two-dimensional phenomenon, the one-dimensional compressor model only captures the effects of rotating stall as a reduced pressure rise. Therefore, a two-dimensional compressor model is used for this study to represent the rotating stall dynamics. In addition, two-dimensional actuation in the form of air injectors will be used for actuation. A gain-scheduling approach is presented for the control of rotating stall subject to wheel speed transients. The operating range of the compressor will be parameterized by wheel speed. At selected discrete wheel speeds within the operating range, a robust feedback controller is designed for each frozen parameter linear model to regulate rotating stall. This set of controllers will then be interpolated over the operating range and scheduled with respect to wheel speed. To illustrate the performance of the feedback system, domains of attraction will be estimated using initial condition simulations.

To this end, the paper contains the following sections. First, the nonlinear analytic compressor model is developed. Then, the problem statement is defined. The linearized spatial domain compressor model is then developed. In the following section the gain-schedule controller design method using the technique of loop shaping in the gain-phase plane is presented. An example is provided to illustrate the design procedure. Finally, the paper ends with conclusions.

II. Analytic Compressor Model: Nonlinear Ordinary Differential Equation

The development of the analytic compressor model, shown in Fig. 2, is based on several works appearing in the open literature. To construct the model, the Moore–Greitzer partial differential equation (PDE) description of an axial flow compressor developed in Refs. 8 and 9 is modified to account for nonconstant wheel speed, unsteady losses, and air injectors as actuators. To account for nonconstant wheel speed, spool dynamics are developed. This results in the Greitzer B parameter becoming a state of the model as described by Gravdahl.[5] The description of the losses is formulated as detailed by Haynes et al.[10] The air injectors are developed as formulated by Hendricks et al.[11]; however, the higher-order nonlinear terms are retained. The modified PDE description of the compressor is then reduced to a nonlinear ordinary differential equation using the method developed by Mansoux et al.[12] Fourier series solutions are used to remove the spatial derivatives. The circumference of the compressor is then discretized to replace the Fourier series with discrete Fourier transforms (DFT), thus, making the model finite dimensional. The number of points in which the annulus of the

Received 4 November 2003; revision received 31 January 2005; accepted for publication 3 March 2005.

*Research Assistant, School of Mechanical Engineering.
†Professor, School of Mechanical Engineering.
‡McAllister Distinguished Professor, School of Mechanical Engineering. Associate Fellow AIAA.

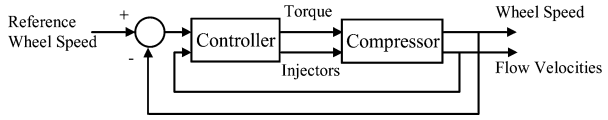

Fig. 1 Block diagram for variable-speed compressor model control system.

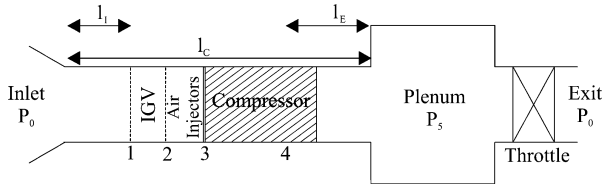

Fig. 2 Compressor.

compressor is discretized determines the number of spatial modes, N, included in the model.

When the following vectors are defined for flow coefficient at the compressor face ϕ_3, the injector flow coefficient ϕ_j, the nondimensional losses across the stator L_s, and the nondimensional losses across the rotor L_r as

$$\boldsymbol{\phi}_3 = \begin{bmatrix} \phi_3(\theta_1) \\ \phi_3(\theta_2) \\ \vdots \\ \phi_3(\theta_{2N+1}) \end{bmatrix} \qquad \boldsymbol{\phi}_j = \begin{bmatrix} \phi_j(\theta_1) \\ \phi_j(\theta_2) \\ \vdots \\ \phi_j(\theta_{2N+1}) \end{bmatrix}$$

$$\boldsymbol{L}_r = \begin{bmatrix} L_r(\theta_1) \\ L_r(\theta_2) \\ \vdots \\ L_r(\theta_{2N+1}) \end{bmatrix} \qquad \boldsymbol{L}_s = \begin{bmatrix} L_s(\theta_1) \\ L_s(\theta_2) \\ \vdots \\ L_s(\theta_{2N+1}) \end{bmatrix} \tag{1}$$

where $\theta_n = 2\pi n/(2N+1)$ and N is a power of 2, the real-valued DFT matrix G that maps the vectors in Eq. (1) into its Fourier coefficients

$$G : \phi \to [\tilde{\phi}_0 \quad \mathrm{Re}(\tilde{\phi}_1) \quad \mathrm{Im}(\tilde{\phi}_1) \quad \cdots \quad \mathrm{Re}(\tilde{\phi}_n) \quad \mathrm{Im}(\tilde{\phi}_n)]^T$$

is given by

$$G = \frac{2}{2n+1}\begin{bmatrix} \frac{1}{\sqrt{2}} & \frac{1}{\sqrt{2}} & \cdots & \frac{1}{\sqrt{2}} \\ \cos(\theta_1) & \cos(\theta_2) & & \cos(\theta_{2N+1}) \\ \sin(\theta_1) & \sin(\theta_2) & & \sin(\theta_{2N+1}) \\ \cos(2\theta_1) & & & \\ \sin(2\theta_1) & & \ddots & \\ \cos(n\theta_1) & \cos(n\theta_2) & \cdots & \cos(n\theta_{2N+1}) \\ \sin(n\theta_1) & \sin(n\theta_2) & \cdots & \sin(n\theta_{2N+1}) \end{bmatrix}$$

When the state vectors in Eq. (1) are used, the variable wheel speed compressor model is given by

where $\bar{\Psi}$ is the nondimensional pressure rise across the compressor, K_T is the throttle parameter, l_c is the effective nondimensional compressor length, l_i is the nondimensional compressor inlet duct length, l_e is the nondimensional compressor exit duct length, λ is the rotor fluid inertia parameter, μ is the compressor fluid inertia parameter, B is the Greitzer B parameter, U is the wheel speed, U_d is the desired wheel speed, A_r is the ratio between injector area and compressor duct area, τ_a is the actuator time constant, τ_{rL} is the loss time constant for the rotor, τ_{sL} is the loss time constant across the stator, Λ is a nondimesional constant inversely proportional to spool inertia, and Γ_c is the torque of the compressor. The inputs to the system are Γ_t, the torque applied to the compressor, and ϕ_{jc}, the injector command. The steady-state losses across the rotor and stator are given by

$$L_{rs}(\phi_3) = (\Psi_{\mathrm{isen}} - \Psi_{\mathrm{css}})R_l \qquad L_{\mathrm{ss}}(\phi_3) = (\Psi_{\mathrm{isen}} - \Psi_{\mathrm{css}})(1 - R_l)$$

respectively, where Ψ_{isen} is the isentropic compressor characteristic, Ψ_{css} is the steady-state compressor characteristic, and R_l is the percentage of the losses across the rotor. In addition, the following vectors and matricies are defined:

$$\Gamma = [1 \quad \cdots \quad 1]^T \qquad S = \begin{bmatrix} \frac{1}{2n+1} & \cdots & \frac{1}{2n+1} \end{bmatrix}$$

$$\boldsymbol{\Psi}_{\mathrm{eff}}(\phi_3, \phi_j) = [\Psi_{\mathrm{eff}}(\phi_3(\theta_1), \phi_j(\theta_1)) \quad \cdots \quad \Psi_{\mathrm{eff}}(\phi_3(\theta_{2N+1}), \phi_j(\theta_{2N+1}))]^T$$

with

$$\Psi_{\mathrm{eff}}[\phi_3(\theta), \phi_j(\theta)] = \Psi_{\mathrm{isen}}[\phi_3(\theta)] + [\phi_j(\theta) - \phi_3(\theta)]A_r\phi_j(\theta) + \frac{1}{2}[A_r\phi_j(\theta)]^2$$

$$E_1 = G^{-1}D_{E1}G$$

$$D_{E1} = \mathrm{diag}\left(l_c, \begin{bmatrix} \left(\frac{2}{l} + \mu\right) & 0 \\ 0 & \left(\frac{2}{l} + \mu\right) \end{bmatrix}, \ldots, \begin{bmatrix} \left(\frac{2}{n} + \mu\right) & 0 \\ 0 & \left(\frac{2}{n} + \mu\right) \end{bmatrix}\right)$$

$$E_2 = G^{-1}D_{E2}G$$

$$D_{E2} = \mathrm{diag}\left(l_i, \begin{bmatrix} 1 & 0 \\ 0 & 1 \end{bmatrix}, \ldots, \begin{bmatrix} \frac{1}{|n|} & 0 \\ 0 & \frac{1}{|n|} \end{bmatrix}\right)$$

$$\begin{bmatrix} \frac{d\bar{\Psi}}{d\xi} \\ E_1\frac{d\phi_3}{d\xi} \\ \frac{d\phi_j}{d\xi} \\ \frac{d\boldsymbol{L}_r}{d\xi} \\ \frac{d\boldsymbol{L}_s}{d\xi} \\ \frac{dU}{d\xi} \end{bmatrix} = \begin{Bmatrix} \frac{U}{U_d}\frac{1}{4l_cB^2}\left(S\phi_3 - K_T\bar{\Psi}^{\frac{1}{2}}\right) - 2\frac{\bar{\Psi}}{U}\frac{dU}{d\xi} \\ \frac{1}{U}\frac{dU}{d\xi}(-E_3\phi_3 + E_2A_r\phi_j) + \frac{U}{U_d}[\bar{\Psi}_{\mathrm{eff}}(\phi_3, \phi_j) - L_r - L_s - \lambda E_4\phi_3 - T\bar{\Psi}] + E_2\frac{d(A_r\phi_j)}{d\xi} \\ \frac{1}{\tau_a}(\phi_{jc} - \phi_j) - \frac{1}{U}\frac{dU}{d\xi}\phi_j \\ \frac{1}{\tau_{rL}}[\boldsymbol{L}_{rs}(\phi_3) - \boldsymbol{L}_r] - \frac{U}{U_d}E_4\boldsymbol{L}_r - \frac{2}{U}\frac{dU}{d\xi}\boldsymbol{L}_r \\ \frac{1}{\tau_{sL}}[\boldsymbol{L}_{\mathrm{ss}}(\phi_3) - \boldsymbol{L}_s] - \frac{2}{U}\frac{dU}{d\xi}\boldsymbol{L}_s \\ \Lambda\frac{U^2}{U_d}(\Gamma_t - \Gamma_c) \end{Bmatrix} \tag{2}$$

Table 1 Compressor model parameters defined at $U = 72$ m/s

Variable	Value	Variable	Value	Variable	Value
$\phi_{3,\text{stall}}$	0.460	R_l	0.75	l_c	6.66
ϕ_j	0.467	τ_{sl}	0.37	l_i	2.99
B	0.1	τ_{rl}	0.37	l_e	2.38
μ	1.29	τ_a	0.1	Λ	0.0603
m	2	λ	0.68	A_r	0.0197

$$E_3 = G^{-1} D_{E3} G$$

$$D_{E3} = \text{diag}\left(l_i + l_e, \begin{bmatrix} 2 & 0 \\ 0 & 2 \end{bmatrix}, \ldots, \begin{bmatrix} \frac{2}{|n|} & 0 \\ 0 & \frac{2}{|n|} \end{bmatrix} \right)$$

$$E_4 = G^{-1} D_{E4} G$$

$$D_{E4} = \text{diag}\left(0, \begin{bmatrix} 0 & 1 \\ -1 & 0 \end{bmatrix}, \ldots, \begin{bmatrix} 0 & n \\ -n & 0 \end{bmatrix} \right)$$

where $\text{diag}(d_1, \ldots, d_n)$ is a block diagonal matrix with $d_1, \ldots, d_n$ on the diagonal.

This model will be used to perform simulations and evaluate the performance of the control law developed. The parameters for the compressor used in this study are listed in Table 1. The compressor model maps are

$$\Psi_{\text{isen}}(\phi) = -15.5341\phi^3 + 24.1238\phi^2 - 15.0262\phi + 4.6951$$

$$\Psi_{\text{css}}(\phi) = \begin{cases} 12.117\phi^2 - 2.423\phi + 0.221 & \phi \le 0.1 \\ -49.624\phi^3 + 39.509\phi^2 - 6.413\phi + 0.395 & 0.1 < \phi \le 0.4 \\ -10.0695\phi^2 + 9.430\phi - 1.184 & 0.4 < \phi \end{cases}$$

These parameters are based on the compressor C2 in Refs. 12 and 13.

III. Problem Statement Development

A. Motivation: Influence of Wheel Speed Transients on Stability

Consider the initial condition response of the compressor resulting from a step change in desired wheel speed. The stability properties that is, domains of attraction of the compressor are related to the rate of change of the wheel speed. To illustrate this, consider the case where the wheel speed control law is given by

$$\Gamma = \Gamma_t - \Gamma_c = K_w(U_d - U) \tag{3}$$

where K_w is the wheel speed control gain, U_d is the desired wheel speed, and U is the actual wheel speed. The resulting wheel speed dynamics captured in Eq. (2) subject to Eq. (3) is

$$\frac{\mathrm{d}U}{\mathrm{d}\xi} = \Lambda \frac{U^2}{U_d} K_w(U_d - U)$$

For comparison, the transient responses are shown in Fig. 3 for two K_w gains, $K_w = 0.0001$ and $K_w = 0.001$, with $U_d = 30$ m/s, initial wheel speed $U_0 = 72$ m/s, and an initial first spatial mode perturbation $|A_1| = 0.02$ with no rotating stall control. The response with the larger K_w, that is, faster wheel deceleration, has a larger flow transient toward the surge line. As a result of this larger flow transient, the compressor enters rotating stall. The effect the faster wheel speed transient has on the stability properties of the compressor is also shown in Fig. 4. As K_w increases, the domains of attraction for a first spatial mode initial condition decreases. Therefore, a tradeoff is made between the stability properties of the compressor and the rate at which the wheel speed may be changed. This gives rise to the control problem of simultaneously controlling wheel speed and rotating to alleviate this tradeoff.

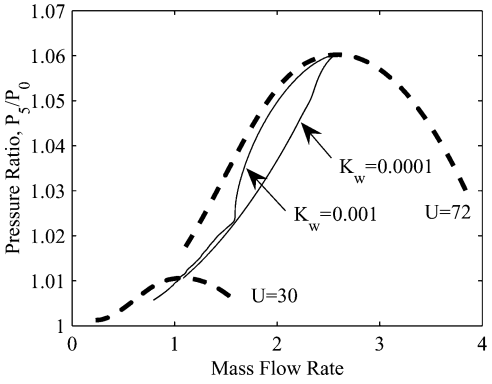

Fig. 3 Transient responses with no rotating stall control for two K_w gains with $U_0 = 72$ and $U_d = 30$.

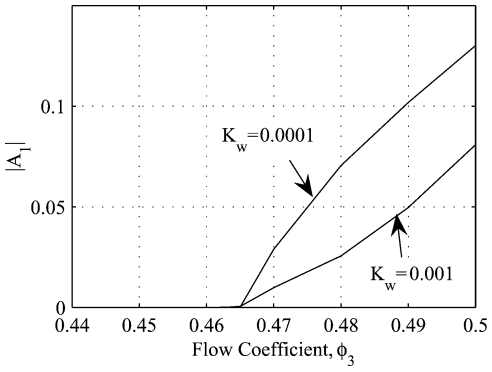

Fig. 4 First spatial mode domain of attraction with no rotating stall control for two K_w gains.

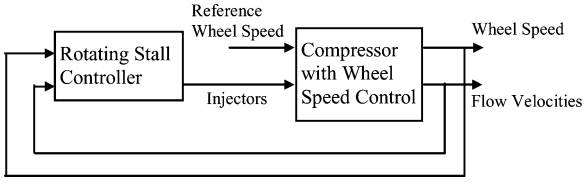

Fig. 5 Block diagram for compressor control system with wheel speed control law Eq. (3).

B. Problem Statement

Shown in Fig. 1 is the multi-input/multi-output block diagram for the simultaneous control of rotating stall and wheel speed. In this study, it will be assumed the wheel speed control law is designed independently of consideration of rotating stall. With a wheel speed control law given, the feedback control system shown in Fig. 1 reduces to the system shown in Fig. 5. The objective is to design a rotating stall control law to improve the stability properties for the compressor system shown in Fig. 5 subject to wheel speed transients. Performance of the control law will be based on an estimation of the domains of attraction obtained from simulated initial condition responses.

IV. Main Result

The problem of rotating stall control is formulated as a nonaxisymmetric flow regulating problem. To facilitate the rotating stall controller design process, the controller design will be performed in the spatial domain. In the spatial domain regulating nonaxisymmetric flow is equivalent to regulating the spatial modes.

A gain-scheduling approach is proposed to accommodate the larger operating range associated with nonconstant wheel speed. This type of methodology is appealing because it separates the controller design process into manageable parts. In this approach, the dynamics associated with the transients of the scheduling variable

are ignored during the design process. Therefore, a family of linear controllers is designed for the frozen parameter systems at the selected operating points to achieve the desired local performance and stability. These local controllers are then interpolated over the operating range and scheduled to form a control law for the operating range considered. Note, because the dynamics of the system associated with the transition between operating points is not explicitly considered, the stability and performance at each operating point does not guarantee stability and performance during the transition between operating points. Therefore, performance and stability of the gain-scheduled control law will be validated through simulation.

Presented in this section is the gain-schedule procedure for the control of rotating stall subject to wheel speed transients. First, the linearized variable wheel speed compressor model is presented. The method for designing the local rotating stall regulating controllers and the scheduling of this set of controllers is then presented. A design example is then given to illustrate the design procedure.

A. Linearized Model of the Compressor

Linearization of the variable wheel speed compressor model presented in Sec. II for the mean flow rate $\bar{\phi}_3$ and mean injection rate $\bar{\phi}_j$ results in the following linear spatial-domain compressor model given by

$$\dot{\boldsymbol{x}}_n(t,\theta) = (F - \Lambda\Gamma F_\Gamma)\boldsymbol{x}_n(t,\theta) + \begin{bmatrix} \dfrac{A_r}{\zeta|n|\tau_a} \\ \dfrac{1}{\tau_a} \\ 0 \\ 0 \end{bmatrix} \hat{u}_n(t,\theta) \qquad (4)$$

$$\hat{y}_n(t,\theta) = [1 \quad 0 \quad 0 \quad 0]\, x_n(t,\theta)$$

where

$$F = \begin{bmatrix} \dfrac{1}{\zeta}\dfrac{U}{U_d}\left(\left.\dfrac{\mathrm{d}\Psi_{\mathrm{isen}}}{\mathrm{d}\phi_3}\right|_{\bar{\phi}_3} - A_r\bar{\phi}_j + in\lambda\right) & -\dfrac{A_r}{\zeta}\dfrac{U}{U_d}(2\bar{\phi}_j - \bar{\phi}_3 + A_r\bar{\phi}_j) - \dfrac{A_r}{\zeta|n|\tau_a} & -\dfrac{1}{\zeta}\dfrac{U}{U_d} & -\dfrac{1}{\zeta}\dfrac{U}{U_d} \\ 0 & -\dfrac{1}{\tau_a} & 0 & 0 \\ \dfrac{1}{\tau_a}\left.\dfrac{\mathrm{d}L_{rs}}{\mathrm{d}\phi_3}\right|_{\bar{\phi}_3} & 0 & \left(\dfrac{U}{U_d}\right)in - \dfrac{1}{\tau_r} & 0 \\ \dfrac{1}{\tau_a}\left.\dfrac{\mathrm{d}L_{\mathrm{ss}}}{\mathrm{d}\phi_3}\right|_{\bar{\phi}_3} & 0 & 0 & -\dfrac{1}{\tau_a} \end{bmatrix}$$

$$F_\Gamma = \mathrm{diag}\left(\frac{2}{|n|}\frac{U}{U_d}, \frac{U}{U_d}, \frac{U}{U_d}, \frac{U}{U_d}\right) \qquad \zeta = \left(\frac{2}{|n|} + \mu\right)$$

$$x_n(t,\theta) = \left[\hat{\phi}_{3_n} \quad \hat{\phi}_{j_n} \quad \hat{L}_{r_n} \quad \hat{L}_{s_n}\right]^T$$

The model in Eq. (4) represents the relationship between the nth spatial mode output and the nth spatial mode input. The input $\hat{u}_n(t) = \hat{\phi}_{jc}$ is the commanded injection rate. The output $\hat{y}_n(t,\theta) = \hat{\phi}_{3_n}$ is the nth spatial harmonic of the flow perturbation at the inlet of the compressor. Note that, if $U = U_d = \text{const}$, then $\Gamma = 0$ and Eq. (4) reduces to the linearized constant wheel speed model.

The linearized model given by Eq. (4) will be used for the design of local linear controllers that will be scheduled. Frequency-response functions will be generated from this model. These frequency responses are used to graphically design the local controllers on the gain-phase plane.

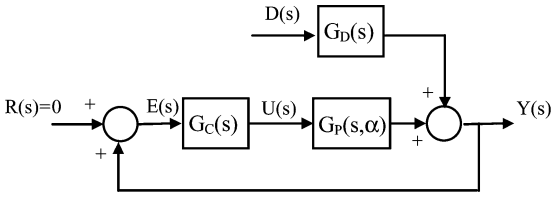

Fig. 6 Block diagram of feedback system.

B. Local Controller Design

With the desired wheel speed U_d given, the linearized model given by Eq. (4) is dependent on two variables, U and $\bar{\phi}_3$. To simplify the gain-schedule control law, the variations in the linearized dynamics with respect to flow coefficient $\bar{\phi}_3$ will be treated as uncertainty in the linear robust control framework. Thus, only wheel speed will be used to schedule the control law. At each selected wheel speed, the frequency responses for the family of mean flow coefficients will be shaped in the gain-phase plane to reduce closed-loop sensitivity. A review of robust linear robust control and the utility of the gain-phase plane follows.

1. Robust Feedback Control Structure and Sensitivity Function

The problem of rotating stall control can be classified as the regulator problem in feedback control systems where nonaxisymmetric flow is to be regulated. Shown in Fig. 6 is a general block diagram with positive feedback. The closed-loop relationship between the inputs and system outputs is

$$Y(s,\alpha) = \frac{G_P(s,\alpha)G_C(s)}{1 - G_P(s,\alpha)G_C(s)}R(s) + \frac{G_D(s)}{1 - G_P(s,\alpha)G_C(s)}D(s)$$

where α is the plant uncertainty. $G_P(s,\alpha)$ is the transfer function equivalence of Eq. (4), where α is the uncertainty in the system dynamics with respect to the flow coefficient. For the rotating stall regulator design, the reference $R(s)$ is equal to zero, that is, axisymmetric flow. Therefore,

$$Y(s,\alpha) = \frac{G_D(s)}{1 - G_P(s,\alpha)G_C(s)}D(s) = S(s,\alpha)G_D(s)D(s) \qquad (5)$$

where $S(s,\alpha) = 1/[1 - L(s,\alpha)]$ is the closed-loop sensitivity function, $L(s,\alpha) = G_P(s,\alpha)G_C(s)$ is the open-loop transfer function to be designed, and $D_0(s) = G_D(s)D(s)$ is the disturbance from the control system point of view.

The goal of a regulating system is to suppress the transmission of the disturbance $D_0(s)$ to the system output $Y(s,\alpha)$ through design

Table 2 Sensitivity regions

Region	$\lvert S(j\omega)\rvert$	Result
1	<1	Attenuation of $\lvert D_0(s)\rvert$
2	$=1$	Attenuation of $\lvert D_0(s)\rvert$
3	>1	Amplification of $\lvert D_0(s)\rvert$

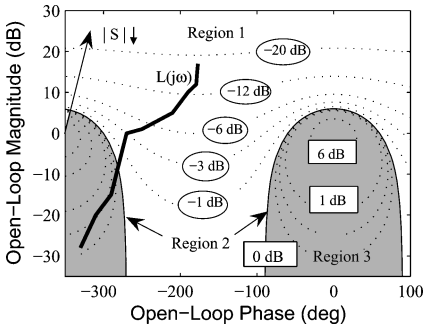

Fig. 7 Gain-phase plane with constant magnitude sensitivity contours.

of a stabilizing controller $G_C(s)$. From Eq. (5), it can be seen that if $S(s,\alpha)=0$, then the external disturbance $D_0(s)$ can be completely rejected. Unfortunately, realizing $S(s,\alpha)=0$ requires an infinite amount of control actuation. Therefore, the control objective is to make $|S(j\omega,\alpha)|<1$ at those frequencies where $D_0(s)$ has significant energy.

2. Gain-Phase Plane with Sensitivity Contours

To design a controller in the frequency domain, designers generally analyze the frequency response of the open-loop system $L(j\omega,\alpha)=G_P(j\omega,\alpha)G_C(j\omega,\alpha)$. The classical approach to a frequency-domain design involves a procedure known as loop shaping and is executed on a Bode plot. For our purposes, the open-loop gain-phase plane will have more controller design utility. The major benefit of the open-loop gain-phase plane is that the closed-loop sensitivity contours can be transparently displayed. Shown in Fig. 7 is the open-loop gain-phase plane with several constant magnitude closed-loop sensitivity contours. Note that three distinct sensitivity regions emerge on the gain-phase plane are listed in Table 2. These regions and sensitivity contours will be used to facilitate the design process.

Consider the case when $L(j\omega_1)$ exists in the disturbance attenuation region of the gain-phase plane. As the open-loop gain $|L(j\omega_1)|$ is increased, $|S(j\omega_1)|$ decreases, leading to better disturbance attenuation. This makes intuitive sense because a higher open-loop gain requires more actuation effort. On the other hand, consider the case when $L(j\omega_1)$ exists in the disturbance amplification region of the gain-phase plane. Here, a decrease in $|L(j\omega_1)|$ leads to a decrease in $|S(j\omega_1)|$, although $|S(j\omega_1)|>1$. Note that closed-loop stability is a prerequisite to performance and can be assessed with the open-loop frequency response by satisfying the correct number of encirclements of the (n360-deg, 0-dB) point in the gain-phase plane as defined by the Nyquist contour and the principle of the argument, where n is an integer. To illustrate the design process an example is presented for the case of constant wheel speed.

3. Constant Wheel Speed Controller Design Example

Consider the constant wheel speed case where $U=U_d=72$ m/s. The objective of the controller is to minimize sensitivity at the disturbance frequencies subject to stabilizing the system. To determine the frequency content of the disturbance, refer to the response of the first spatial mode to a throttle input shown in Fig. 8. As shown in Fig. 8, the amplitude of the first spatial mode begins to grow slowly for $\xi\approx 11{,}380$, then abruptly develops in a fully developed rotating stall cell. During this growth, the phase angle is approximately a line with constant slope of 0.33. Thus, the first spatial mode disturbance is rotating at approximately a single frequency of 0.33. Therefore minimizing the sensitivity at this frequency will attenuate

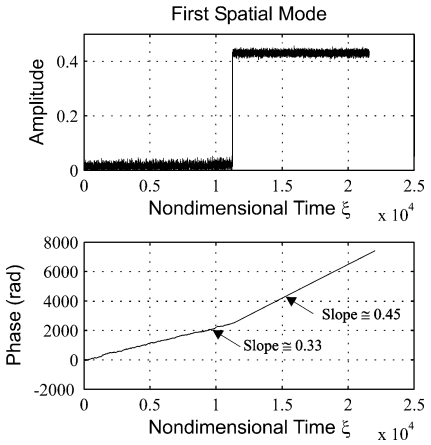

Fig. 8 Transient response of first spatial mode to ramp throttle input.

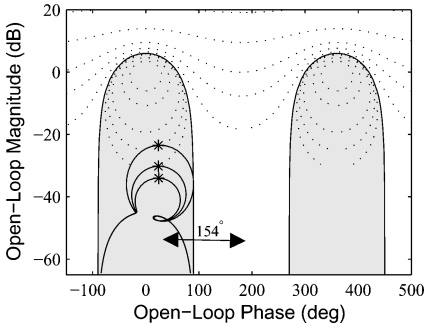

Fig. 9 Set of uncompensated frequency responses: ∗, frequency of 0.33.

the disturbance, preventing or delaying the onset of rotating stall. The design objective is to design $G_C(j\omega)$ such that the open-loop transfer function $L(j\omega,\alpha)$ at $\omega=0.33$ is centered in the disturbance attenuation region of the open-loop gain-phase plane (unshaded region, Fig. 8), thus, achieving the largest sensitivity reduction for the smallest open-loop gain. Knowing the frequency content of the disturbance also identifies the required bandwidth of the actuator because the actuator must react to a disturbance frequency of 0.33.

Shown in Fig. 9 are the frequency-response functions in the open-loop gain-phase plane with the frequency of 0.33 denoted by asterisks. Notice that, for $G_C(j\omega)=1$, $L(j\omega,\alpha)=G_P(j\omega,\alpha)$ resides in the disturbance amplification region of the open-loop gain-phase plane. By inspection of $G_P(j\omega,\alpha)$, it can be seen that the design objective of achieving the largest sensitivity reduction for a given open-loop gain can be achieved by shifting the open-loop frequency responses into the sensitivity reduction region of the gain-phase plane. This can be achieved with a complex gain, $G_C(s)=K_1\exp(j\beta_1)$. The required phase shift that moves $L(j\omega,\alpha)$ such that $S(j0.33,\alpha)$ is minimized for a given open-loop gain is $\beta_1=154$ deg. The gain K_1 is chosen to be 20 for this example. The resulting $L(j\omega,\alpha)$ is shown in Fig. 10.

Because a complex gain control law evolved from the design process, it is simple to compare the results of the controller design with the set of controllers $G_C(s)=20\exp(j\beta_1)$, where $\beta_1\in(0{,}360$ deg). The comparison is made by performing an exhaustive search over the range of possible controller phase shifts. To validate the controller, simulations were performed with controller phase angles from $\beta_1=0$ to $\beta_1=360$ deg at 10-deg increments. Each simulation had a ramp throttle command. The results are shown in Fig. 11. From the simulations, the optimal controller has a phase angle of $\beta_1\approx 150$ deg. The predicted optimal phase angle selection correlates well with the simulated results. Therefore, the use of sensitivity in the gain-phase plane provided a method in designing a controller for rotating stall control.

Also note in Fig. 11 the phase angles $\beta_1\approx 62$ and $\beta_1\approx 240$ deg have no increase in performance over the uncontrolled case. The

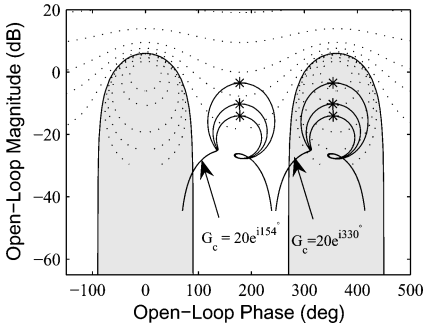

Fig. 10 Set of compensated frequency responses for predicted best and worst performance: ∗, frequency of 0.33.

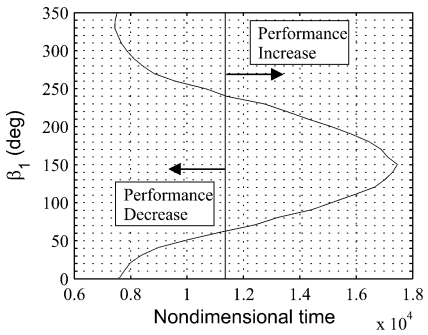

Fig. 11 Contour plot for amplitude of first spatial mode for various controller phase angles β.

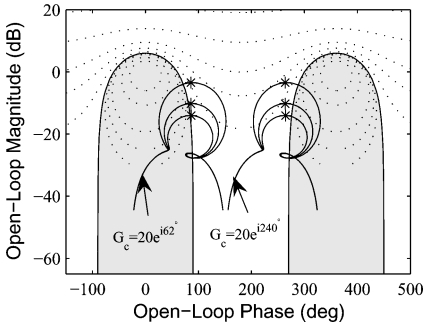

Fig. 12 Compensated frequency responses corresponding to no gain in performance: ∗, frequency of 0.33.

frequency responses with controllers for these two phase angles are plotted in Fig. 12. Notice the proximity to the 0-dB sensitivity contour ($|S(j\omega)| = 1$). This shows the transition from increase in performance to decrease in performance as the frequency responses move toward larger magnitude sensitivity contours

Figure 11 also shows that the controller with $\beta_1 \approx 330$ deg exhibited the worst performance. The frequency responses $L(j\omega, \alpha)$ with this controller are in Fig. 10. This result is expected because the controller maximizes $S(j0.33)$ in the disturbance amplification region. This method will be utilized to design controllers for the frozen parameter compressors models during the gain-scheduling procedure.

C. Scheduling the Local Controllers

With the set of local controllers designed, the gain-scheduled control law is obtained by interpolation between the set of local controllers with respect to wheel speed. The performance and stability of the gain-schedule control law will be validated with estimated domains of attractions obtained through initial condition simulation of the complete nonlinear model.

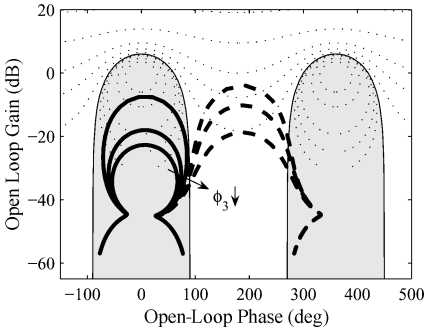

a) Open-loop plants

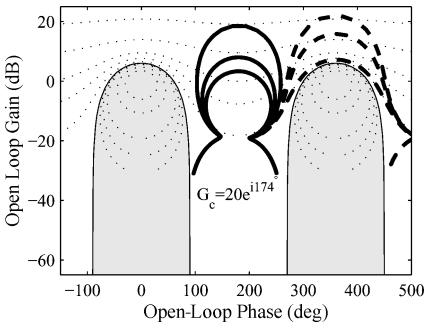

b) Open-loop plants with controller

Fig. 13 Open-loop system for $\bar{\phi}_3 = 0.49, 0.48, 0.47, 0.463, 0.46$, and 0.45 with $U = 30$ m/s and $K_w = 0.001$: ——, stable and – – –, unstable.

D. Design Example

To illustrate the gain-schedule design process, consider the case where the wheel speed control law is given by Eq. (3) with $K_w = 0.001$, $U_0 = 72$ m/s, and $U_d = 30$ m/s. The compressor parameters used for this example are defined in Table 1 and in the model maps. The operating range to be parameterized by wheel speed is $U \in [30, 72]$ m/s. Selecting several operating points in this range is the next step in the procedure. For this example, four points are chosen: $U = 30$, 44, 58, and 72 m/s. At each of these discrete operating points, a local control law is designed to regulate the first spatial mode for the linearized spatial-domain compressor model Eq. (4). When the method developed for the constant wheel speed case is used, controllers will be designed to reduce the sensitivity for the closed-loop system at each of the selected wheel speeds.

1. Local Controller Design

Consider the case for $U = 30$ m/s (Fig. 13). Shown in Fig. 13a are the first spatial mode frequency responses for $\bar{\phi}_3 = 0.49$, 0.48, 0.47, 0.463, 0.46 and 0.45 for $U = 30$ m/s. Notice that the open-loop stable frequencies responses reside in the shaded area (Fig. 13), the region where closed-loop sensitivity is greater then one. In addition, the frequency responses of the unstable plant do not encircle the positive one point. The objective of the local control law is to shape the frequency responses into the unshaded area, the region where the closed-loop sensitivity is less then one. Also in the case when the open-loop dynamics are unstable, the control law must also shape the frequency response to encircle the positive one point to satisfy the Nyquist encirclement condition for a positive feedback system. As shown in Fig. 13b, the gain-phase plane simplifies the design process by graphically revealing that the complex gain control law, $\hat{u}_1 = 20\exp(j174\text{ deg})\hat{y}_1$, is sufficient to reduce the closed-loop sensitivity for the uncertain plant set by shifting the stable open-loop frequency responses into the unshaded area. In addition, this control law stabilizes the unstable plants by encircling the positive one point. Similarly, the control law $\hat{u}_1 = 20\exp(j\beta)\hat{y}_1$ with $\beta(U = 44\text{ m/s}) = 170$, $\beta(U = 58\text{ m/s}) = 166$, and $\beta(U = 72\text{ m/s}) = 164$ deg achieves sensitivity reduction for the other selected wheel speeds, respectively. These values are summarized in Table 3.

Table 3 Controller phase at each selected wheel speed

U, m/s	β, deg
30	174
44	170
58	166
72	164

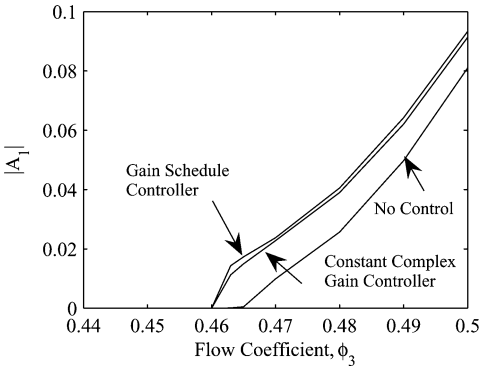

Fig. 14 First spatial mode domain of attraction with gain-schedule controller, constant complex gain controller, and without rotating stall controller for $K_w = 0.001$.

2. Scheduling the Control Laws

With the local rotating stall controllers designed for the discrete operating points, the next step is to interpolate these control laws over the entire operating range. Notice that the only parameter in the rotating stall control law that varies with will respect to wheel speed is β. Therefore, β is the only variable to be scheduled. The controller phase is interpolated by fitting a polynomial using least squares. For this example, a third-order polynomial was chosen. The resulting scheduled control law is $\hat{u}_1 = 20\exp[j\beta(U)]\hat{y}_1$, where

$$\beta(U) = 0.000121U^3 - 0.0160U^2 + 0.396U + 173.27$$

3. Assessing Performance

To assess the performance and stability of the design, the following domains of attraction are shown in Fig. 14 for $K_w = 0.001$. The control law improved the stability of the compressor subject to wheel speed transients. Also for comparison, the domains of attraction for the constant complex gain control law $\hat{u}_1 = 20\exp(j174\,\text{deg})\hat{y}_1$ is designed for $U_d = U = 30$ m/s. Both the gain-scheduled law and the constant complex gain control law improve the compressor stability properties; however, the gain-scheduled law achieves better performance at the cost of using an additional feedback signal for scheduling.

V. Conclusions

Presented in this paper is a gain-scheduling approach for the control of rotating stall subject to wheel speed transients. The benefit of the gain-schedule approach is that it simplifies the design process by separating the controller design process into manageable parts. This allows for the utility of using linear robust design techniques such as loop shaping on the gain-phase plane. To reduce the complexity of the scheduled control law, $\bar{\phi}_3$ is treated as uncertainty. The method of linear robust spatial-domain control of rotating stall is used to design the local control laws.

In the design example, a simple complex gain controller was shown to be sufficient to reduce the closed-loop sensitivity at each of the selected discrete wheel speeds. In addition, the control structure resulting from the local designs were the same. This simplifies the scheduling of the control law. These complex gain control laws are then scheduled through interpolation to form the gain-schedule control law. The resulting rotating stall control was shown to expand the domain of attraction and achieve better performance then a constant complex gain control law.

References

[1]Cohen, H., Rogers, G. F. C., and Saravanamuttoo, H. I. H., *Gas Turbine Theory*, 3rd ed., Longman Scientific and Technical, Essex, England, U.K., 1987.

[2]Khalil, H. K., *Nonlinear Systems*. Prentice–Hall, NJ, 1996, Chaps. 11, 13.

[3]Shamma, J. S., and Athans, M., "Analysis of Gain Scheduled Control for Nonlinear Plants," *IEEE Transactions on Automatic Control*, Vol. 35, No. 8, 1990, pp. 898–907.

[4]Rugh, W. J., and Shamma, J. S., "Survey Paper: Research on Gain Scheduling," *Automatica*, Vol. 36, No. 10, 2000, pp. 1401–1425.

[5]Gravdahl, J. T., "Modeling and Control of Surge and Rotating Stall in Compressors," Ph.D. Dissertation, Dept. of Engineering Cybernetics, Norwegian Univ. of Science and Technology, Norway, March 1998.

[6]Leonessa, A., Haddad, W. M., and Li, H., "Global Stabilization of Centrifugal Compressors via Stability-based Switching Controllers," *Proceedings of the 1999 IEEE International Conference on Control Applications*, IEEE Publications, Piscataway, NJ, 1999, pp. 1383–1388.

[7]Badmus, O. O., Nett, C. N., and Schork, F. J., "An Integrated, Full-Range Surge Control/Rotating Stall Avoidance Compressor Control System," *Proceedings of the American Control Conference*, Vol. 3, IEEE Publications, Piscataway, NJ, 1991, pp. 3173–3180.

[8]Moore, F. K., and Greitzer, E., "A Theory of Post-Stall transients in Axial Compression Systems: Part I—Development of Equations," *Journal of Engineering for Gas Turbines and Power*, Vol. 108, Jan. 1986, pp. 68–76.

[9]Moore, F. K., "A Theory of Rotating Stall of Multistage Axial Compressors: Part I—Small Disturbances," *Journal of Engineering for Gas Turbines and Power*, Vol. 106, April 1984, pp. 313–320.

[10]Haynes, J., Hendricks, G., and Epstein, A., "Active Stabilization of Rotating Stall in a Three-Stage Axial Compressor," *Journal of Turbomachinery*, Vol. 116, April 1994, pp. 226–239.

[11]Hendricks, G., and Gysling, D., "Theoretical Study of Sensor–Actuator Schemes for Rotating Stall Control," *Journal of Propulsion and Power*, Vol. 10, No. 1, 1994, pp. 101–109.

[12]Mansoux, C., Gysling, D., Setiawan, J., and Paduano, J., "Distributed Nonlineare Modeling and Stability Analysis of Axial Compressor Stall and Surge," *Proceedings of the American Control Conference*, IEEE Publications, Piscataway, NJ, 1994, pp. 2305–2316.

[13]Protz, J. M., "Nonlinear Active Control of Rotating Stall and Surege," M.S. Thesis, Dept. of Aeronautics and Astronautics, Massachusetts Inst. of Technology, Cambridge, MA, June 1997.